PROCEEDINGS OF SPIE

Design of an optimized graphene plasmonic splitter utilizing higher-order mode propagation

Amanatiadis, Stamatios, Kantartzis, Nikolaos

SPIE.

Design of an optimized graphene plasmonic splitter utilizing higher-order mode propagation

Stamatios A. Amanatiadis[a] and Nikolaos V. Kantartzis[a]

[a]Department of Electrical and Computer Engineering, Aristotle University of Thessaloniki, GR-54124 Thessaloniki, Greece

ABSTRACT

The efficient stimulation of a graphene microstrip plasmonic splitter via higher-order mode propagation is proposed in the current work. Initially, graphene waveguiding systems are investigated thoroughly in terms of the supported propagating modes and their potential excitation. Specifically, the microstrip apparatus is examined focusing on the distribution of bulk modes. This analysis indicates that the transition of a higher-order mode to a lower one is potentially smooth if an appropriately selected microstrip width is utilized. Consequently, an effective graphene plasmonic device is designed and stimulated via a higher-order bulk mode that equally splits the propagating surface wave to separated microstrips. The latter supports a lower-order mode and it is evaluated that the undesired back-reflected waves are minimized. Moreover, a thorough performance analysis is numerically conducted by means of a flexible Finite-Difference Time-Domain algorithm validating the remarkable functionality at a wide frequency range.

Keywords: Dispersion curve, effective index, FDTD, FEM, microstrip, modal solver, surface conductivity

1. INTRODUCTION

During the past decade, graphene attracted significant attention to the research community due to its exotic properties.[1] Despite its negligible thickness, graphene presents finite conductivity leading to notable phenomena such as the ability to support highly confined transverse magnetic (TM) surface plasmon polariton (SPP) waves.[2,3] The latter are, mainly, observed at millimeter-wave and THz frequencies, thus enabling the development of various devices for advanced applications. The plasmonic waveguiding systems, including graphene microstrips, constitute one of the most important class of devices and their propagation properties have been investigated comprehensively.[4,5] In particular, a graphene microstrip supports various propagating plasmonic modes, separated into two major categories, the edge and the bulk ones in respect to the electromagnetic field concentration.[6–8] The proper manipulation of the aforementioned attributes facilitates the optimized design of auxiliary apparatuses including plasmonic splitters, namely the main focus of this paper.

Plasmonic splitters are important parts of a complete electromagnetic system due to their significance to divide propagating electromagnetic waves. Various graphene implementations have been proposed utilizing the propagation properties on microstrips. Specifically, complex structures have been designed as beam dividers of the edge modes,[9] while the latter are analyzed, also, via theoretical aspects of the transmission line theory.[10] Moreover, the effect of chemical potential has been studied for the beam splitting adjustment,[11,12] while a multimode interference-based approach has been tested for small perturbations of the geometry.[13,14] Finally, the surface wave manipulation via graphene metasurfaces indicated interesting properties as a power divider.[15]

In our work, a novel graphene surface wave splitter is proposed utilizing a higher-order mode propagation in a simple microstrip structure. Initially, the attributes of the supported electromagnetic modes on graphene microstrips are reviewed, highlighting that the higher-order bulk modes are concentrated in specific portions of the microstrip. Consequently, the transition towards a plasmonic waveguide with an appropriately selected width is a straightforward procedure. The proper width selection is, also, realized via the examination of the

---

Further author information: (Send correspondence to Stamatios Amanatiadis)
Stamatios Amanatiadis: E-mail: samanati@auth.gr
Nikolaos Kantartzis: E-mail: kant@auth.gr

surface wave propagation properties since it is intended to retain the effective index during the transition to minimize the undesired reflected waves. This preliminary analysis reveals broadband characteristics, while the effectiveness of our design is evaluated numerically through an accurate Finite-Difference Time-Domain (FDTD) scheme that treats graphene as an equivalent surface current. The extracted full-wave results successfully validate the performance of the plasmonic splitter at a wide frequency range.

2. THEORETICAL ANALYSIS OF SURFACE WAVES ON GRAPHENE

Throughout our analysis, graphene is considered as an infinitesimally thin, local two-sided layer, characterized by an isotropic surface conductivity $\sigma(\omega, \mu_c, \Gamma, T)$, where ω is the radian frequency, μ_c the chemical potential controlled by a gate voltage or chemical doping, Γ a phenomenological scattering rate assumed to be independent of energy, and T the temperature. In this framework, the conductivity is evaluated through the subsequent expression resulting from the Kubo formula[16]

$$\sigma_g(\omega, \mu_c, \Gamma, T) = je^2 \frac{(\omega - j2\Gamma)}{\pi \hbar^2} \left[\frac{1}{(\omega - j2\Gamma)^2} \int_0^\infty \varepsilon \left(\frac{\partial f_d(\varepsilon)}{\partial \varepsilon} - \frac{\partial f_d(-\varepsilon)}{\partial \varepsilon} \right) \mathrm{d}\varepsilon \right.$$
$$\left. - \int_0^\infty \frac{f_d(-\varepsilon) - f_d(\varepsilon)}{(\omega - j2\Gamma)^2 - 4(\varepsilon/\hbar)^2} \mathrm{d}\varepsilon \right], \tag{1}$$

with $-e$ the electron's charge, $\hbar$ the reduced Planck's constant, $f_d = [e^{(\varepsilon - \mu_c)/k_B T} + 1]^{-1}$ the Fermi-Dirac distribution, and k_B the Boltzmann's constant. The interband contributions, i.e. the second term of (1), are negligible compared to the intraband one, implying the first term at the examined frequency range and can be ignored simplifying graphene's conductivity to the reduced expression,

$$\sigma_{\mathrm{intra}}(\omega, \mu_c, \Gamma, T) = \frac{e^2 k_B T}{\pi \hbar^2 (j\omega + 2\Gamma)} \left[\frac{\mu_c}{k_B T} + 2 \ln \left(e^{-\mu_c/k_B T} + 1 \right) \right]. \tag{2}$$

In this context, the complex wavenumber of the SPP wave k_ρ of free-standing graphene is theoretically computed in terms of the surface conductivity through[3]

$$k_\rho = k_0 \sqrt{1 - \left(\frac{2}{\eta_0 \sigma_g} \right)^2} = n_{\mathrm{eff}} k_0, \tag{3}$$

where k_0 and η_0 are the free-space wavenumber and wave-impedance, respectively and n_{eff} is the effective index of the surface wave. The latter is defined as the the normalized SPP wavenumber to the free-space one and it is an important factor since it facilitates the intuitive comparison between different propagating modes.

3. GRAPHENE MICROSTRIP SUPPORTED MODES

The previous analysis considered a graphene layer of infinite dimensions that is not practical for waveguiding systems. For this reason, finite-width graphene microstrips are designed and their analysis requires numerical
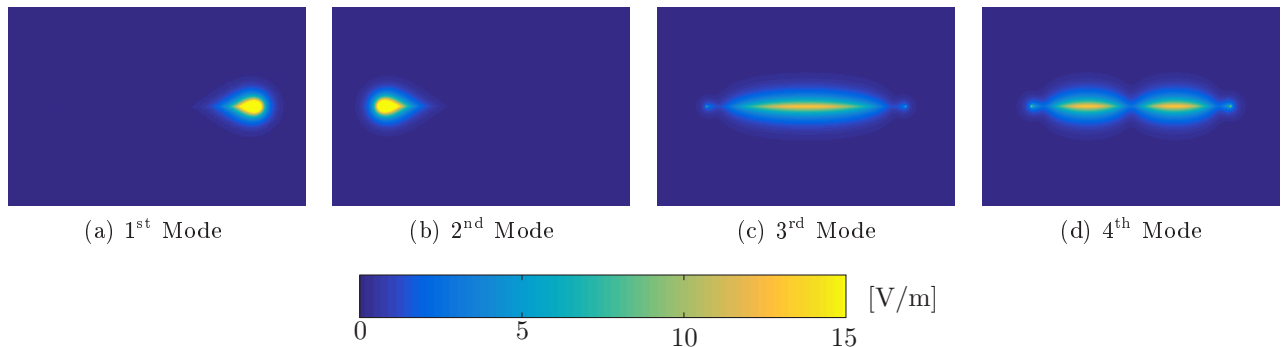

(a) 1$^{\mathrm{st}}$ Mode   (b) 2$^{\mathrm{nd}}$ Mode   (c) 3$^{\mathrm{rd}}$ Mode   (d) 4$^{\mathrm{th}}$ Mode

Figure 1. Electric field distribution of the initial four modes to a $20\,\mu$m-wide graphene microribbon at $3\,$THz.
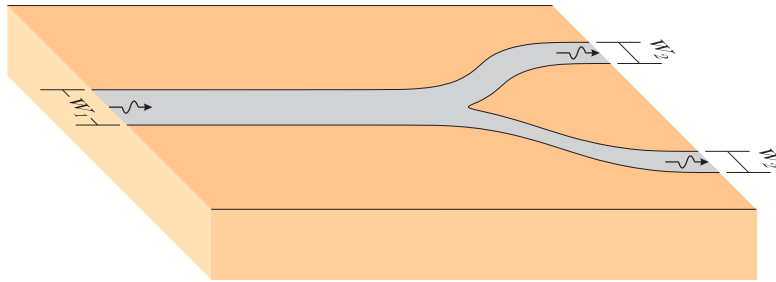
Figure 2. The proposed setup of a graphene plasmonic splitter.

solutions for the evaluation of the propagating modes. In this work, an efficient modal solver, based on the Finite Element Method, is utilized with graphene modeled as an equivalent surface current. Then, a quadratic eigenvalue problem is solved to extract directly the effective index of each propagating mode on the microstrip.[17] In this paper, a $20\,\mu$m-wide microstrip is considered, while the chemical potential of graphene is selected $0.1\,$eV, the scattering rate $0.33\,$meV at the far-infrared spectrum.

The electric field distribution of the first four modes is depicted in Fig. 1 and the separation into edge and bulk modes is evident via the observation of the electric field concentration. Moreover, the initial bulk mode coincides with the third microstrip one, while as the order is increased, the concentration is distributed equally in different portions of the microstrip. In particular, the fourth mode, Fig. 1d, presents two different concentration regions and a minimum is observed at the center of the waveguide in contrast to the third mode.

This interesting phenomenon is exploited in our work, and a simple geometry, illustrated in Fig. 2, is designed as a graphene plasmonic splitter. Here, it is intended to stimulate the main w_1-wide microstrip via the fourth mode expecting a straightforward separation of the surface wave to the narrower w_2-wide microstrips that support third mode propagation. Although this procedure is relatively simple, a complete dispersion analysis is required to select appropriately the width for a successful transition of the SPP wave.

Initially, the main microstrip, of $w_1 = 20\,\mu$m width, is investigated in terms of the first four modes dispersion curves, sketched in Fig. 3. An important observation is the absence of a cut-off frequency for the first mode, while both edge modes present higher effective indices compared to the bulk ones due to the increased concentration of the electrons near the edges. Moreover, the bulk modes exhibit larger cut-off frequencies, and their effective indices converge to the infinite layer one as the surface wave wavelength is significantly lower compared to the microstrip width. This paper focuses on the stimulation of the fourth mode with a cut-off frequency at approximately $2.6\,$THz. However, the propagation losses are significant near cut-off and they are stabilized at a satisfactory level beyond $3\,$THz, thus this is the operational limit of the proposed device.

Now, the main purpose is to identify the width w_2 of the separated microstrips that supports a third mode propagation with an effective index identical to the fourth mode of the initial $20\,\mu$m-wide plasmonic waveguide.
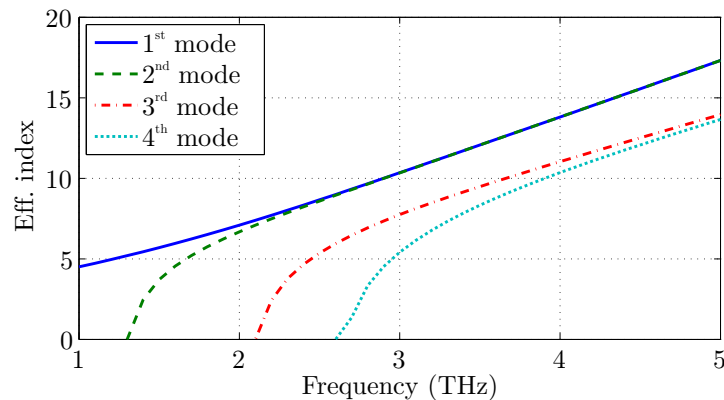

Figure 3. Dispersion curves of the first four modes on a $20\,\mu$m-wide graphene microstrip.
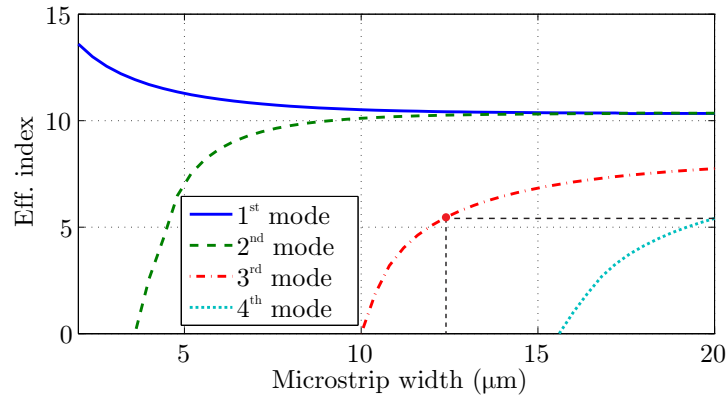
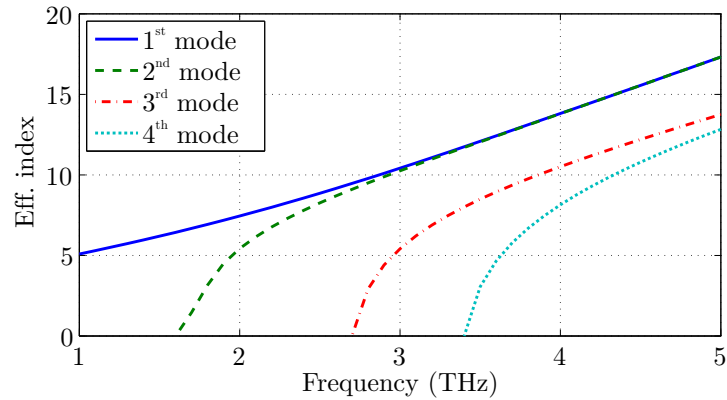Figure 4. Surface wave effective index versus graphene microstrip width for the first four modes at 3 THz.

Figure 5. Dispersion curves of the first four modes on a 12.35 μm-wide graphene microstrip.

The appropriate width w_2 is investigated via a parametric analysis of the effective index versus the microstrip dimensions. To this end, this relation is extracted at 3 THz and it is demonstrated in Fig. 4. Similarly to the dispersion diagram, the first mode is propagating independently to the width, while the bulk modes are available for wider microstrips. Additionally, the desired width is explicitly highlighted in Fig. 4 and it corresponds to the value 12.35 μm.

The dispersion analysis of this narrower 12.35 μm-wide microstrip is, also, extracted and depicted in Fig. 5. Although the dispersion characteristics are equivalent to the 20 μm-wide device, the cut-off frequencies are shifted towards a higher spectrum. Furthermore, in Fig. 6 is conducted a comparison between the involved modes of
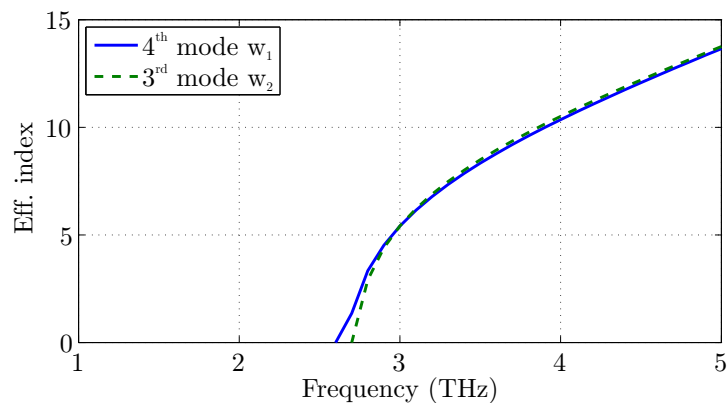

Figure 6. Dispersion curve comparison between the 3rd and the 4th mode on a $w_1 = 20\,\mu$m and $w_2 = 12.35\,\mu$m, respectively, wide graphene microstrip.

our analysis, namely the fourth and the third modes of the microstrips with $w_1 = 20\,\mu$m and $w_2 = 12.35\,\mu$m width, respectively. An important feature is revealed via this comparison since the dispersion curves are almost identical, especially beyond 3 THz. As a consequence, a potentially smooth transition is achieved for a wide range of frequencies.

4. PERFORMANCE VALIDATION OF THE GRAPHENE SPLITTER

The performance of the proposed higher-order mode graphene plasmonic splitter is numerically validated via a full-wave analysis utilizing the popular FDTD method. Particularly, the conventional algorithm is appropriately modified to accurately model graphene as an equivalent surface current.[18] The proposed setup of Fig. 2 is designed width $w_1 = 20\,\mu$m and $w_2 = 12.35\,\mu$m, based on the previous analysis, while graphene parameters are $\mu_c = 0.1\,$eV and $\Gamma = 0.33\,$meV. The computational domain is divided in $320 \times 400 \times 200$ cells of $\Delta x = \Delta y = \Delta z = 0.5\,\mu$m and the time-step is set to $\Delta t = 0.8\,$fs. Finally, open boundaries are terminated via an 8-cell thick Perfectly Matched Layer (PML).

Initially, the electric field distribution is extracted in Fig. 7 for stimulation of the main microstrip via the third and the fourth mode. It is evident that the transition of the fourth mode (Fig. 7b) to the splitter branches is sufficiently smooth in contrast to the third one (Fig. 7a). However, the quantitative characterization is realized
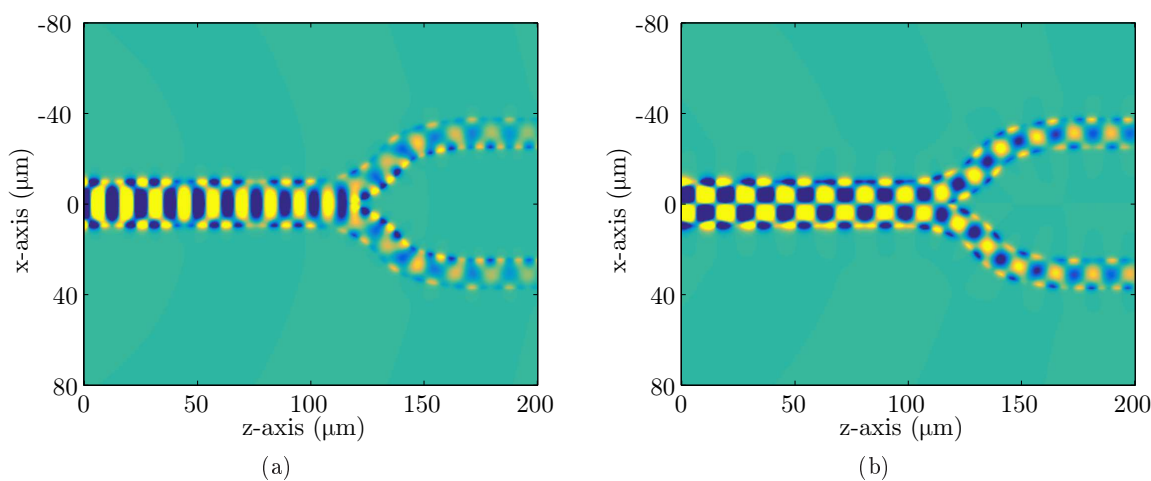

Figure 7. Distribution of the normal, to graphene, electric field component, E_y, for (a) $3^{\rm rd}$ and (b) $4^{\rm th}$ mode propagation on the main graphene microstrip.
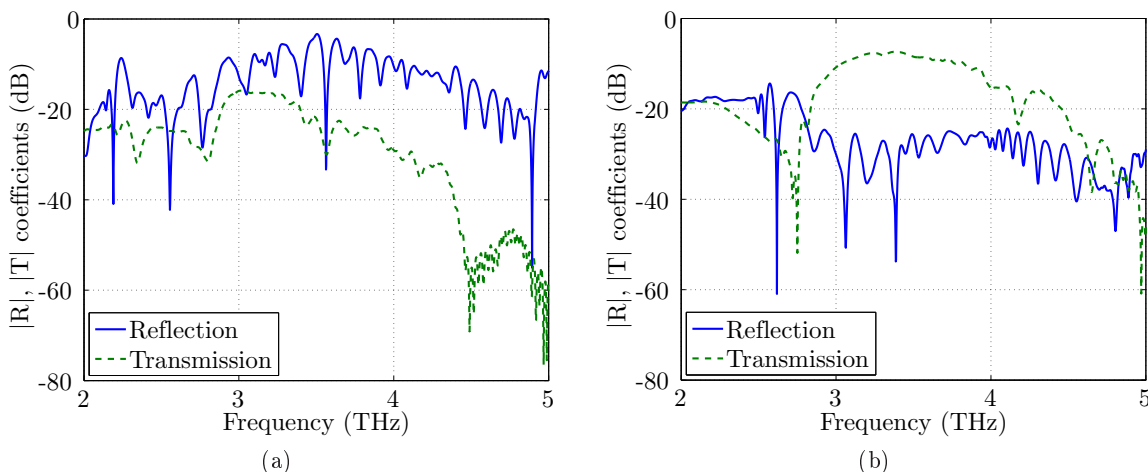

Figure 8. Reflection and transmission coefficients of the proposed graphene splitter for (a) $3^{\rm rd}$ and (b) $4^{\rm th}$ mode propagation on the main microstrip.

via the extraction of the reflection and transmission coefficients in Fig. 8. It is worth mentioning that the former is measured $20\,\mu$m before the splitter branches, while the latter is evaluated at the exit point of the device.

Initially, the stimulation of the device via the third mode, Fig. 8a, presents increased reflected waves since the $5\,$dB level is exceeded at several frequencies. For this reason, the transmitted wave towards the splitter branches is severely degraded with a maximum value of $-16\,$dB at approximately $3\,$THz. Nevertheless, this behavior is inverted via a fourth mode stimulation of the main microstrip. Specifically, the reflection coefficient is retained below $-20\,$dB beyond $3\,$THz, while the surface wave is efficiently transmitted for a wide frequency range, namely $3-4\,$THz. Note a local minimum is observed at $2.6\,$THz that coincides to the cut-off frequency of this mode, thus, the transmission below this point is due to the edge modes. Furthermore, the transmission beyond $4\,$THz is decreased significantly due to the propagation losses of graphene. Finally, all the extracted results validate the remarkable performance of the proposed graphene plasmonic spitter.

5. CONCLUSION

A novel graphene plasmonic splitter stimulated via a higher-order microstrip mode, has been proposed and thoroughly analyzed in this paper. The modal analysis on graphene waveguiding systems indicated that a proper selection of microstrip widths enables a smooth transition between different propagating bulk modes. Then, the proposed device has been investigated through an efficient FDTD method that treats graphene accurately as an equivalent surface current. The numerical results validated successfully that a fourth mode stimulation provides an exceptional surface wave splitting performance at a broadband frequency range.

ACKNOWLEDGMENTS

REFERENCES

[1] Geim, A. K. and Novoselov, K. S., "The rise of graphene," in [*Nanoscience and technology: a collection of reviews from nature journals*], 11–19, World Scientific (2010).

[2] Mikhailov, S. A. and Ziegler, K., "New electromagnetic mode in graphene," *Physical review letters* **99**(1), 016803 (2007).

[3] Hanson, G. W., "Dyadic green's functions and guided surface waves for a surface conductivity model of graphene," *Journal of Applied Physics* **103**(6), 064302 (2008).

[4] Kim, J. T. and Choi, S.-Y., "Graphene-based plasmonic waveguides for photonic integrated circuits," *Optics express* **19**(24), 24557–24562 (2011).

[5] Xu, W., Zhu, Z., Liu, K., Zhang, J., Yuan, X., Lu, Q., and Qin, S., "Dielectric loaded graphene plasmon waveguide," *Optics express* **23**(4), 5147–5153 (2015).

[6] Zhang, F.-M., He, Y., and Chen, X., "Guided modes in graphene waveguides," *Applied Physics Letters* **94**(21), 212105 (2009).

[7] Nikitin, A. Y., Guinea, F., García-Vidal, F., and Martín-Moreno, L., "Edge and waveguide terahertz surface plasmon modes in graphene microribbons," *Physical Review B* **84**(16), 161407 (2011).

[8] Forati, E. and Hanson, G. W., "Soft-boundary graphene nanoribbon formed by a graphene sheet above a perturbed ground plane: conductivity profile and spp modal current distribution," *Journal of optics* **15**(11), 114006 (2013).

[9] Rezaei, M. H. and Zarifkar, A., "Subwavelength electro-optical half-subtractor and half-adder based on graphene plasmonic waveguides," *Plasmonics* **14**(6), 1939–1947 (2019).

[10] Zhu, X., Yan, W., Mortensen, N. A., and Xiao, S., "Bends and splitters in graphene nanoribbon waveguides," *Optics Express* **21**(3), 3486–3491 (2013).

[11] Ooi, K. J., Chu, H. S., Ang, L. K., and Bai, P., "Mid-infrared active graphene nanoribbon plasmonic waveguide devices," *JOSA B* **30**(12), 3111–3116 (2013).

[12] Yang, J., Xin, H., Han, Y., Chen, D., Zhang, J., Huang, J., and Zhang, Z., "Ultra-compact beam splitter and filter based on a graphene plasmon waveguide," *Applied optics* **56**(35), 9814–9821 (2017).

[13] Deng, Q., Liu, L., Li, X., and Zhou, Z., "Arbitrary-ratio 1×2 power splitter based on asymmetric multimode interference," *Optics letters* **39**(19), 5590–5593 (2014).

[14] Qiu, P., Qiu, W., Lin, Z., Chen, H., Tang, Y., Wang, J., Kan, Q., and Pan, J., "Ultra-compact tunable graphene-based plasmonic multimode interference power splitter in mid infrared frequencies," *Science China Information Sciences* **60**(8), 082402 (2017).

[15] Chorsi, H. T. and Gedney, S. D., "Tunable plasmonic optoelectronic devices based on graphene metasurfaces," *IEEE Photonics Technology Letters* **29**(2), 228–230 (2016).

[16] Gusynin, V., Sharapov, S., and Carbotte, J., "Magneto-optical conductivity in graphene," *Journal of Physics: Condensed Matter* **19**(2), 026222 (2006).

[17] Demirtzioglou, I. and Yioultsis, T., "Analysis of graphene plasmonic waveguides and switching components via a finite element formulation with surface conductivity," in [*PIERS Proceedings*], 6–9 (2015).

[18] Amanatiadis, S. A., Zygiridis, T. T., and Kantartzis, N. V., "Combining standard with optimised split-step finite-difference time-domain methods for the study of graphene configurations," *IET Science, Measurement & Technology* **13**(8), 1150–1157 (2019).